symmetry

MDPI

Article

Solution of Water and Sodium Alginate-Based Casson Type Hybrid Nanofluid with Slip and Sinusoidal Heat Conditions: A Prabhakar Fractional Derivative Approach

Ali Raza [1,2], Musawa Y. Almusawa [3], Qasim Ali [1], Absar Ul Haq [4], Kamel Al-Khaled [5] and Ioannis E. Sarris [6,*]

1 Department of Mathematics, University of Engineering and Technology, Lahore 54890, Pakistan
2 Department of Mathematics, Minhaj University, Lahore 54770, Pakistan
3 Department of Mathematics, Faculty of Science, Jazan University, Jazan 45142, Saudi Arabia
4 Department of Basic Science and Humanities, Narowal Campus, University of Engineering and Technology, Lahore 54890, Pakistan
5 Department of Mathematics & Statistics, Jordan University of Science and Technology, P.O. Box 3030, Irbid 22110, Jordan
6 Department of Mechanical Engineering, University of West Attica, 250 Thivon & P. Ralli Str., 12244 Athens, Greece
* Correspondence: sarris@uniwa.gr

check for updates

Citation: Raza, A.; Almusawa, M.Y.; Ali, Q.; Haq, A.U.; Al-Khaled, K.; Sarris, I.E. Solution of Water and Sodium Alginate-Based Casson Type Hybrid Nanofluid with Slip and Sinusoidal Heat Conditions: A Prabhakar Fractional Derivative Approach. *Symmetry* **2022**, *14*, 2658. https://doi.org/10.3390/sym14122658

Academic Editor: Alessandro Sarracino

Received: 29 October 2022
Accepted: 5 December 2022
Published: 15 December 2022

Abstract: This paper aims to investigate free convection heat transmission in hybrid nanofluids across an inclined pours plate, which characterizes an asymmetrical hybrid nanofluid flow and heat transfer behavior. With an angled magnetic field applied, sliding on the border of walls is also considered with sinusoidal heat transfer boundary conditions. The non-dimensional leading equations are converted into a fractional model using an effective mathematical fractional approach known as the Prabhakar time fractional derivative. Silver (Ag) and titanium dioxide (TiO_2) are both considered nanoparticles, with water (H_2O) and sodium alginate ($C_6H_9NaO_7$) serving as the base fluids. The solution of the momentum, concentration, and energy equation is found by utilizing the Laplace scheme, and different numerical algorithms are considered for the inverse of Laplace, i.e., Stehfest and Tzou's. The graphical analysis investigates the impact and symmetry of significant physical and fractional parameters. Consequently, we surmise that water-based hybrid nanofluid has a somewhat higher velocity than sodium alginate-based hybrid nanofluid. Furthermore, the Casson parameter has a dual effect on the momentum profile. Furthermore, the memory effect reduces as fractional restriction increases for both the velocity and temperature layers. The results demonstrate that increasing the heat transmission in the solid nanoparticle volume fractions enhanced the heat transmission. In addition, the numerical assessment examined the increase in mass and heat transmission, while shear stress was increased with an increase in the Prabhakar fractional parameter α.

Keywords: heat transfer; Prabhakar derivative; slip; Casson fluid; sodium alginate

1. Introduction

During previous years, various attempts have been made to attain the actual thermal effectiveness of diverse systems. This is part of these attempts to enhance the thermal transfer rate by adding different nanoparticles and mixed convection flow [1,2]. The effect of a mixed convection MHD flow along with diverse Grashof numbers, Reynolds numbers, and Hartmann numbers are examined by Al-Salem et al. [3]. They observed that heat convection and flow speed are affected by the path of fluid motion and permit the magnetic field, which sources a deprived transfer of heat. Furthermore, Lorentz's force in the reverse flow direction is produced using a magnetic force. Another form of nanofluid (NF) that has newly received consideration is known as the hybrid nanofluid (HNF). Simultaneous mixtures of a metallic nanoparticle and a non-metallic form increase the thermal conduction and solidity of the NF [4]. Using this, the characteristics of two or three nanoparticles may be utilized. As yet, several investigations have been made on HNFs. The effects of Al_2O_3-Cu-H_2O and Al_2O_3-H_2O are differentiated through Moghadassi et al. [5]. They determined that the transfer of convective heat is far advanced in the case of HNF. Suresh et al. [6] discussed the viscosity and thermal conductivity of hybrid (Al_2O_3-Cu-H_2O) nano-suspension in a cylinder. They exposed that transfer of heat is elevated when the HNF is utilized. Singh et al. [7] used the quasi-linearization method with an implicit finite difference technique to study the mixed convection flow along a vertical plate. Govindaraj et al. [8] discussed the MHD NF flow over an accelerated vertical plate with different viscosity values and Prandtl numbers. Gnanaprasanna et al. [9] numerically examined a mathematical flow model of Casson NF over a flat plate.

Further, the laminar flow through a hot cylinder filled with HNF (Al_2O_3-Cu-H_2O) was investigated empirically by Suresh et al. [10] and exhibited that the Nusselt number is enlarged in an HNF in contrast with pure water. The HNF (Ag-MgO-H_2O) through a square cavity was premeditated by Ghalambaz et al. [11]. The impacts of disparity of the major constraints, such as the nanoparticle volume fraction, were considered. The impact on the entropy construction and MHD convection of HNF Al_2O_3-Cu in a permeable square addition was deliberated by a numerical scheme in [12]. They noted that heat transmission in convection mode increases by increasing Rayleigh number while it decreases with the increase in Hartmann number. Non-Newtonian fluids are fluids that do not have a linear relationship between rates of deformation and stress. Non-Newtonian fluids are used in a wide range of scientific and technology sectors, such as crude oil extraction and fiber varnishing, and have piqued the interest of many researchers. Because of their flexibility, non-Newtonian fluids do not have all of their characteristics explained in a single equation. Casson fluid, commonly known as a shear-thinning liquid, is a non-Newtonian fluid. Casson-type fluids include honey, human blood, tomato sauce jelly, and others. Casson fluids are studied by engineers, mathematicians, biomedical researchers, and scientists due to their diverse uses. Because of this phenomenon and in nature, several types are established. The Casson model is an important model that is established, and this fluid model explains yield stress. The Casson NF model with the impact of the magnetic field was studied in [13]. A model of non-Newtonian NF because of heat transference in the existence of a porous surface by taking the stagnation point was deliberated by Nadeem et al. [14]. The Casson NF model with the impacts of MHD and heat transfer was inspected by Haq et al. [15]. Alwawi et al. [16] explored the Casson NF model and heat transference produced by the Lorentz force. The water-based boundary layer flow over a stretching surface along with a vertical plate was discussed by employing the Quasilinearization scheme by Govindaraj et al. [17]. The boundary layer flow in a diverging channel along with diverse viscosity was solved numerically with the quasilinearization method [18]. Patil et al. [19] investigated the MHD triple diffusing quadratic and convective Eyring–Powell NF flow over a vertical plate in diffusing liquid oxygen and hydrogen by employing the implicit finite difference estimation. Iyyappan et al. [20] investigated the boundary layer forced convection flow in a diverging channel with viscous dissipation and heat source/sink on momentum and temperature fields numerically. Patil et al. [21] examined a mathematical model of heat and mass transfer in the nonlinear convective Williamson NF with a moving plate. The shape effects of MHD nanoparticles were studied on energy and fluid flow features on a slender cylinder by employing the implicit finite difference system and quasi-linearization technique [22]. The mixed convective HNF flow around a yawed cylinder with one type of nanoparticle was investigated by utilizing the quasilinearization and the finite method [23].

We see that a numerical model involving an integer-order derivative, with the non-linear model, cannot work suitably in many cases. Fractional calculus has numerous implementations in electromagnetics, viscoplasticity, fluid mechanics, fluid dynamics, processing of signals, as well as optics. It is exploited to explain the model's physics and design forms formulated through fractional approaches. The Caputo fractional derivative

(CTFD) with the utilization of time-fractional distribution by employing a fast method for variable order was discussed by Fang et al. [24]. Ali et al. [25] investigated HNFs with continuous reasonable CTFD due to a pressure gradient. A mathematical model demonstrating the human liver with Caputo–Fabrizio derivatives (CF) was studied by Baleanu et al. [26]. Atangana–Baleanu derivatives (AB) are a novel utilization for designing an AB-fractional mask image dispensation communicated in [27]. Saqib et al. [28] examined the heat transfer rate of CNTs-based nanofluid moving on an inclined plate without singular and local kernels definitions of fractional derivatives. In [29], authors investigate the MHD channel flow of BTF containing hybrid nanoparticles with the help of nonlocal definitions of recent fractional derivatives. Moreover, the recent work completed on different steady and unsteady flows can be seen in [30–34]. The heat transfer fractional study based on AB and CF derivatives for MHD mixed convection flow with nanoparticles (copper oxide and silver) through an inclined moving surface using the Laplace method was completed by Bafakeeh et al. [35]. Sadiq et al. [36] used the Laplace approach to investigate the natural convection heat transfer NF fractional model with CF derivative inside a channel with ramped wall conditions under the impacts of radiation, chemical reactions, and the Soret effect.

In 1971, the Prabhakar work was proposed by an Indian mathematician, Professor Tilak Raj Prabhakar, who anticipated a generality of the Mittag–Leffler function involving three parameters. Using the Prabhakar derivative along with precise fractional coefficients might be a valuable path for choosing suitable numerical models that are recognized as a good arrangement between trial and hypothetical outcomes [37,38]. Due to massive uses in fluid mechanics, researchers studied fractional models based on Caputo, CF, AB, and Prabhakar's time-fractional derivatives to study the memory effects of different Newtonian and non-Newtonian models in [39–44]. The carbon nanotube NF, along with Prabhakar-type thermal transport and free convection flow, was deliberated by Elnaqeeb et al. [45]. Shah et al. [46] discussed a Prabhakar fractional of Maxwell fluid with thermal transport and free convection flow model. Raza et al. [47] used the Laplace method to examine viscous natural convection fractionalized fluid flowing based on Prabhakar fractional operator with slip effects, constant mass diffusion, and Newtonian heating over an oscillating inclined plate. Asjad et al. [48] used the Prabhakar operator to obtain a fractional problem of Jeffrey fluid along a moving vertical plate and the equations for energy, and the Laplace approach solved momentum. Recent definitions of fractional derivatives can be seen in [40,49–51].

In the literature, researchers dismissed the notion of fractional, particularly the Prabhakar form fractional, which has an extended Mittag–Leffler function as its kernel and can regulate the momentum and thermal boundary layers. This research investigates the mixed convection heat transfer in HNFs across an inclined vertical plate. With an angled magnetic field applied, sliding on the border of walls is also considered. The non-dimensional controlling equations are converted into a fractional model using an effective mathematical fractional method known as the Prabhakar time-fractional derivative. Silver (Ag) and titanium dioxide (TiO_2) are nanoparticles with water and sodium alginate as base fluids. The Laplace scheme is used to solve the momentum, concentration, and energy equation, and several numerical approaches are studied for the inverse of Laplace. The graphical depiction also discusses the effects of physical and flow characteristics.

2. Mathematical Formulation

Assume an unsteady free convection nanofluid mixed with silver (Ag) and titanium dioxide (TiO_2) as nanoparticles. Furthermore, water (H_2O) and sodium alginate ($C_6H_9NaO_7$) are considered as a base fluid of flowing hybrid nanofluid on an inclined plate with ambient temperature T_∞. Moreover, a magnetic field of intensity B_o^2 provided to the poured plate at an angle of inclination θ_1. Because of the low Reynolds number values, the induced magnetic field is neglected. At the start of time $t = 0$, the system is at rest, and the fluid is also motionless with a constant temperature. After some time $t > 0^+$, the system begins to oscillate with some constant velocity $H(t)Cos(\omega t)$, and the hybrid nanofluid begins to flow across the plate owing to oscillations of the inclined plane, as shown in Figure 1.

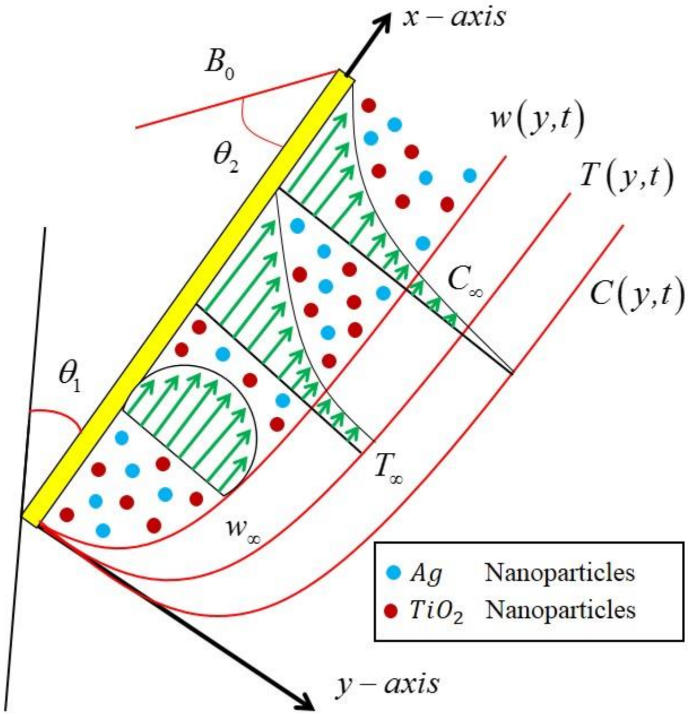

Figure 1. Physical flow.

As a result of the assumptions mentioned above and the Boussinesq's approximation [52], the significant leading governing equations of free convection-flowing fluid may be described as [53].

The momentum field:

$$\begin{aligned}\rho_{nf}\frac{\partial w_{(y,t)}}{\partial t} = \left(1+\frac{1}{\Lambda_0}\right)\frac{\partial^2 w_{(y,t)}}{\partial y^2} - \left(\sigma_{nf}B_o^2 Sin(\theta_1) + \left(1+\frac{1}{\Lambda_0}\right)\frac{\mu_{nf}}{k}\right)w_{(y,t)} \\ +g(\rho\beta_T)_{nf}\left(T_{(y,t)} - T_\infty\right)Cos(\theta_2) \\ +g(\rho\beta_C)_{nf}\left(C_{(y,t)} - T_\infty\right)Cos(\theta_2)\end{aligned} \tag{1}$$

The energy equation:

$$\left(\rho C_p\right)_{nf}\frac{\partial T_{(y,t)}}{\partial t} = -\frac{\partial \delta_{(y,t)}}{\partial y}, \text{where } \delta_{(y,t)} = -k_{nf}\frac{\partial T_{(y,t)}}{\partial y} \tag{2}$$

Concentration field:

$$\frac{\partial C_{(y,t)}}{\partial t} = -\frac{\partial \mathfrak{M}_{(y,t)}}{\partial y}, \text{ where } \mathfrak{M}_{(y,t)} = -D\frac{\partial C_{(y,t)}}{\partial y}. \tag{3}$$

With equivalent conditions:

$$\begin{aligned} w_{(0,t)} - h\left.\frac{\partial w}{\partial y}\right|_{y=0} &= U_o H(t) Cos(\omega t),\ T_{(y,t)} \\ &= \begin{cases} T_\infty + (T_w - T_\infty)\frac{t}{t_o}, & 0 < t \le t_o \\ T_w, & t > t_o \end{cases},\ C_{(0,t)} = C_w \\ w_{(y,t)} \to 0,\ T_{(y,t)} \to T_\infty,&\quad C_{(y,t)} \to C_\infty \quad ;\ y \to \infty,\quad t > 0 \end{aligned}$$

Introducing the consequent non-dimensional variables:

$$w^* = \frac{w}{U_o},\ y^* = \frac{U_o}{v_f}y,\ t^* = \frac{t}{t_o},\quad t_o = \frac{v_f}{U_o^2},\quad T^* = \frac{T_{(y,t)} - T_\infty}{T_w - T_\infty}$$
$$C^* = \frac{C_{(y,t)} - C_\infty}{C_w - C_\infty},\qquad q^* = \frac{q}{q_o}$$

By discarding the static notation in Equations (1)–(3) and comparable conditions, the non-dimensional form of the preceding equations will emerge as

$$\lambda_o \frac{\partial w_{(y,t)}}{\partial t} = \frac{\lambda_1}{\Lambda_1}\frac{\partial^2 w_{(y,t)}}{\partial y^2} - \left(\lambda_2 M Sin(\theta_1) + \frac{\lambda_1}{k}\right) w_{(y,t)} + \lambda_3 Gr T_{(y,t)} Cos(\theta_2) + \lambda_4 Gr C_{(y,t)} Cos(\theta_2) \tag{4}$$

$$\lambda_5 Pr \frac{\partial T_{(y,t)}}{\partial t} = -\frac{\partial \delta_{(y,t)}}{\partial y},\ \delta_{(y,t)} = -\frac{\partial T_{(y,t)}}{\partial y} \tag{5}$$

$$\lambda_6 Sc \frac{\partial C_{(y,t)}}{\partial t} = -\frac{\partial \mathfrak{M}_{(y,t)}}{\partial y},\ \mathfrak{M}_{(y,t)} = -\frac{\partial C_{(y,t)}}{\partial y} \tag{6}$$

With the following transformed conditions:

$$w_{(y,0)} = 0,\qquad T_{(y,0)} = 0,\qquad C_{(y,0)} = 0;\qquad \forall y \geq 0 \tag{7}$$

$$w_{(0,t)} - \mathrm{h}\frac{\partial w}{\partial y}\Big|_{y=0} = H(t)Cos(\omega t),\quad T_{(y,t)} = \begin{cases} t, & 0 < t \leq 1 \\ 1, & t > 1 \end{cases},\qquad C_{(0,t)} = 1 \tag{8}$$

$$w_{(y,t)} \to 0,\quad T_{(y,t)} \to 0,\qquad C_{(y,t)} \to 0\quad ;\quad y \to \infty,\ t > 0 \tag{9}$$

Tables 1 and 2 shows the thermal properties and properties of under-conversation nanoparticles and fluids.

Table 1. The thermal characteristics of nanoparticles and base fluid.

Material	Water (H_2O)	Sodium Alginate ($C_6H_9NaO_7$)	Silver (Ag)	Titanium Dioxide (TiO_2)
$\rho(M/L^3)$	997.1	898	10,500	425
$C_p(J/M\,K)$	4179	4175	235	6862
$k(W/L\,K)$	0.613	0.6367	429	8.9538
$\beta_T(K^{-1})$	21	23	1.89	0.9
σ	0.05	0.07	3.6×10^7	1×10^{-7}

Where:

$$\lambda_o = (1-\varphi) + \varphi\frac{\rho_s}{\rho_f},\qquad \lambda_1 = \frac{1}{(1-\varphi)^{2.5}},\qquad \lambda_2 = 1 + \frac{3\left(\frac{\sigma_s}{\sigma_f} - 1\right)\varphi}{\left(\frac{\sigma_s}{\sigma_f} + 2\right) - \left(\frac{\sigma_s}{\sigma_f} - 1\right)\varphi}$$

$$\lambda_3 = (1-\varphi) + \varphi\frac{(\rho\beta_T)_s}{(\rho\beta_T)_f},\quad \lambda_4 = (1-\varphi) + \varphi\frac{(\rho\beta_C)_s}{(\rho\beta_T)_f}\quad \lambda_5 = \frac{k_{nf}}{k_f},\qquad \Lambda_1 = \frac{\Lambda_0 v_f}{U_o^2}$$

$$Pr = \left(\frac{\mu C_p}{\kappa}\right)_f,\qquad Gr = \frac{g(\rho\beta_T)_f(T_w - T_\infty)}{U_o^3},\quad Sc = \frac{\nu}{D},\qquad Gm = \frac{g(\rho\beta_C)_f(C_w - C_\infty)}{U_o^3}$$

As a result, the equivalent fractional model for the Fourier law of heat conductivity and Fick's law in terms of Prabhakar time-fractional derivatives is as follows

$$\delta_{(y,t)} = -{}^{C}\mathfrak{D}^{\gamma}_{\alpha,\beta,\alpha}\frac{\partial T_{(y,t)}}{\partial y} \tag{10}$$

$$\mathfrak{M}_{(y,t)} = -{}^{C}\mathfrak{D}^{\gamma}_{\alpha,\beta,\alpha}\frac{\partial C_{(y,t)}}{\partial y} \tag{11}$$

where ${}^{C}\mathfrak{D}^{\gamma}_{\alpha,\beta,\alpha}$ is the regularised Prabhakar fractional operator with the necessary preliminaries stated below.

Table 2. Model for thermophysical characteristics of NFs quantities.

Thermal Features	Regular Nanofluid	Hybrid Nanofluid
Density	$\rho_f = \frac{\rho_{nf}}{(1-\varphi)+\varphi\frac{\rho_s}{\rho_s}}$	$\rho_f = \frac{\rho_{hnf}}{\left((1-\varphi_2)\left((1-\varphi_1)+\varphi_1\frac{\rho_{s1}}{\rho_f}\right)+\varphi_2\rho_{s2}\right)}$
Dynamic Viscosity	$\mu_f = \mu_{nf}(1-\varphi)^{2.5}$	$\mu_f = \mu_{hnf}(1-\varphi_1)^{2.5}(1-\varphi_2)^{2.5}$
Electrical Conductivity	$\sigma_f = \frac{\sigma_{nf}}{\left(1+\frac{3\left(\frac{\sigma_s}{\sigma_f}-1\right)\varphi}{\left(\frac{\sigma_s}{\sigma_f}+2\right)-\left(\frac{\sigma_s}{\sigma_f}-1\right)\varphi}\right)}$	$\sigma_{bf} = \frac{\sigma_{hnf}}{\left(1+\frac{3\varphi\left(\varphi_1\sigma_1+\varphi_2\sigma_2-\sigma_{bf}(\varphi_1+\varphi_2)\right)}{\left(\varphi_1\sigma_1+\varphi_2\sigma_2+2\varphi\sigma_{bf}-\varphi\sigma_{bf}\left(\varphi_1\sigma_1+\varphi_2\sigma_2-\sigma_{bf}(\varphi_1+\varphi_2)\right)\right)}\right)}$
Thermal Conductivity	$k_f = \frac{k_{nf}}{\left(\frac{k_s+(n-1)k_f-(n-1)\left(k_f-k_s\right)\varphi}{k_s+(n-1)k_f+\left(k_f-k_s\right)\varphi}\right)}$	$k_{bf} = \frac{k_{hnf}}{\left(\frac{k_{s2}+(n-1)k_{bf}-(n-1)\left(k_{bf}-k_{s2}\right)\varphi_2}{k_{s2}+(n-1)k_{bf}+\left(k_{bf}-k_{s2}\right)\varphi_2}\right)}$ and $k_f = \frac{k_{bf}}{\left(\frac{k_{s1}+(n-1)k_f-(n-1)\left(k_f-k_{s1}\right)\varphi_1}{k_{s1}+(n-1)k_f+\left(k_f-k_{s1}\right)\varphi_1}\right)}$
Heat Capacitance	$(\rho C_p)_f = \frac{(\rho C_p)_{nf}}{(1-\varphi)+\varphi\frac{(\rho C_p)_s}{(\rho C_p)_f}}$	$(\rho C_p)_s = \frac{(\rho C_p)_{hnf}}{(1-\varphi_2)\left((1-\varphi_1)+\varphi_1\frac{(\rho C_p)_{s1}}{(\rho C_p)_f}\right)+\varphi_2(\rho C_p)_{s2}}$
Thermal Expansion Coefficient	$(\rho\beta)_f = \frac{(\rho\beta)_{nf}}{(1-\varphi)+\varphi\frac{(\rho\beta)_s}{(\rho\beta)_f}}$	$(\rho\beta)_f = \frac{(\rho\beta)_{hnf}}{(1-\varphi_2)\left((1-\varphi_1)+\varphi_1\frac{(\rho\beta)_{s1}}{(\rho\beta)_{f1}}\right)+\varphi_2(\rho\beta)_{s2}}$

Definition 1. *The mathematical form of Prabhakar fractional kernel* [54]

$$e^{\gamma}_{\alpha,\beta}(\alpha;t) = t^{\beta-1}E^{\gamma}_{\alpha,\beta}(\alpha t^{\alpha}), \quad Re(\alpha) > 0$$

Definition 2. *The mathematical representation of Prabhakar integral*

$$E^{\gamma}_{\alpha,\beta,\alpha}h(t) = h(t) * e^{\gamma}_{\alpha,\beta}(\alpha;t) = \int_0^t h(\tau)(t-\tau)^{\beta-1}E^{\gamma}_{\alpha,\beta}\left(\alpha(t-\tau)^{\alpha}\right)d\tau$$

with its Laplace transform

$$\mathcal{L}\left\{E^{\gamma}_{\alpha,\beta,\alpha}h(t)\right\}(q) = \mathcal{L}\{h(t)\}\left(\frac{q^{\alpha\gamma-\beta}}{(q^{\alpha}-\alpha)^{\gamma}}\right)$$

Definition 3. *The regularized Prabhakar derivative is distinct as* [55]

$${}^{C}\mathfrak{D}^{\gamma}_{\alpha,\beta,\alpha}h(t) = \int_0^t h^{n}(\tau)(t-\tau)^{n-\beta-1}E^{-\gamma}_{\alpha,n-\beta}\left(\alpha(t-\tau)^{\alpha}\right)d\tau$$

with its Laplace transform

$$\mathcal{L}\left\{{}^{C}\mathfrak{D}^{\gamma}_{\alpha,\beta,\alpha}h(t)\right\} = q^{\beta-n}\left(1-\alpha q^{-\alpha}\right)^{\gamma}\mathcal{L}\{h^{n}(t)\}$$

3. Solution of the Problem

The LT approach is used to solve this issue for both leading equations.

3.1. Energy Profile

By applying the LT to Equations (5) and (10) and inserting Equation (10) into Equation (5), we obtain the ordinary differential equation as follows for the solution of the energy equation.

$$\lambda_5 Pr\, q\, \overline{T}_{(y,q)} = \left(q^{\beta}\left(1-\alpha q^{-\alpha}\right)^{\gamma}\right)\frac{d^2\overline{T}}{dy^2}$$

After simplifying this ordinary differential equation, we yield the general solution with transformed boundary conditions as follows:

$$\overline{T}_{(y,q)} = Ae^{y\sqrt{\frac{\lambda_5 Pr\, q^{1-\beta}}{(1-\alpha q^{-\alpha})^{\gamma}}}} - Be^{-y\sqrt{\frac{\lambda_5 Pr\, q^{1-\beta}}{(1-\alpha q^{-\alpha})^{\gamma}}}} \tag{12}$$

$$\overline{T}_{(0,q)} = \frac{1-e^{-q}}{q^2}, \qquad \overline{T}_{(\infty,q)} = 0$$

Using these conditions, the answer to the thermal equation will be as follows:

$$\overline{T}_{(y,s)} = \frac{1-e^{-q}}{q^2}e^{-y\sqrt{\frac{\lambda_5 Pr\, q^{1-\beta}}{(1-\alpha q^{-\alpha})^{\gamma}}}} \tag{13}$$

The Laplace inverse of Equation (13) will be derived numerically in Table 3.

Table 3. Numerical analysis of governed profiles by both numerical algorithms.

y	$T_{(y,t)}$ **by Stehfest**	$T_{(y,t)}$ **by Tzou's**	$C_{(y,t)}$ **by Stehfest**	$C_{(y,t)}$ **by Tzou's**	$w_{(y,t)}$ **by Stehfest**	$w_{(y,t)}$ **by Tzou's**
0.1	0.8141	0.8215	0.8342	0.8339	1.1816	1.1923
0.3	0.5591	0.5637	0.5802	0.5797	1.2916	1.3035
0.5	0.3840	0.3868	0.4038	0.4029	1.3134	1.3254
0.7	0.2636	0.2653	0.2808	0.2800	1.2777	1.2894
0.9	0.1810	0.1820	0.1593	0.1946	1.2069	1.2108
1.1	0.1243	0.1248	0.1359	0.1352	1.1165	1.1268
1.3	0.0853	0.0856	0.0945	0.0940	1.0169	1.0263
1.5	0.0585	0.0587	0.0658	0.0654	0.9153	0.9237
1.7	0.0402	0.0402	0.0458	0.0454	0.8163	0.8234
1.9	0.0275	0.0275	0.0319	0.0316	0.7223	0.720

3.2. Concentration Profile

We obtain the ordinary differential equation for the simulations of the concentration profile by using the LT on Equations (6) and (11)

$$\lambda_6\, Sc\, q\, \overline{C}_{(y,q)} = -\frac{\partial\overline{\mathfrak{M}}}{\partial y} \tag{14}$$

$$\overline{\mathfrak{M}}_{(y,q)} = -\left(q^{\beta}\left(1-\alpha q^{-\alpha}\right)^{\gamma}\right)\frac{\partial\overline{C}_{(y,q)}}{\partial y} \tag{15}$$

We introduce Equation (15) into Equation (14) and utilize the corresponding conditions we obtain:

$$\overline{C}_{(y,q)} = \frac{1}{q}e^{-y\sqrt{\frac{\lambda_6\ Sc\ q^{1-\beta}}{(1-\alpha q^{-\alpha})^{\gamma}}}} \tag{16}$$

The Laplace inverse of the concentration as mentioned above field solution will be computed numerically in Table 3 using Stehfest and Tzou's techniques.

3.3. Momentum Profile

We use the LT on the modified governing Equation (4) and its following conditions to obtain the momentum profile solution.

$$\frac{\partial^2\ \overline{w}_{(y,q)}}{\partial y^2} - \frac{\Lambda_1}{\lambda_1}\left(\lambda_2 Msin(\theta_1) + \frac{\lambda_1}{k} + \lambda_0 q\right)\overline{w}_{(y,q)} = -\frac{\lambda_3 Gr\Lambda_1 Cos(\theta_2)}{\lambda_1}\overline{T}_{(y,q)} - \frac{\lambda_4 Gr\Lambda_1 Cos(\theta_2)}{\lambda_1}\overline{C}_{(y,q)} \tag{17}$$

$$\overline{w}_{(0,q)} - h\left.\frac{\partial\overline{w}}{\partial y}\right|_{y=0} = \frac{q}{\omega^2+q^2}, \qquad \overline{w}_{(\infty,q)} \to 0$$

Using these circumstances, we obtain the momentum profile simulation shown below.

$$\begin{aligned}
&\overline{w}_{(y,q)} \\
&= \frac{1}{1+h\sqrt{\frac{\Lambda_1}{\lambda_1}\left(\lambda_2 Msin(\theta_1)+\frac{\lambda_1}{k}+\lambda_0 q\right)}}\left(\frac{\lambda_3 Gr\ \Lambda_1\ Cos(\theta_2)\left(1-e^{-q}\right)}{\lambda_1 q^2}\frac{1+h\sqrt{\frac{\lambda_5 Pr\ q}{q^{\beta}(1-\alpha q^{-\alpha})^{\gamma}}}}{\left(\frac{\lambda_5 Pr\ q}{q^{\beta}(1-\alpha q^{-\alpha})^{\gamma}}\right)-\frac{\Lambda_1}{\lambda_1}\left(\lambda_2 Msin(\theta_1)+\frac{\lambda_1}{k}+\lambda_0 q\right)}\right. \\
&\left.+\frac{\lambda_4 Gm\ \Lambda_1\ Cos(\theta_2)}{\lambda_1 q}\frac{1+h\sqrt{\frac{\lambda_6 Sc\ q}{q^{\beta}(1-\alpha q^{-\alpha})^{\gamma}}}}{\left(\frac{\lambda_6 Sc\ q}{q^{\beta}(1-\alpha q^{-\alpha})^{\gamma}}\right)-\frac{\Lambda_1}{\lambda_1}\left(\lambda_2 Msin(\theta_1)+\frac{\lambda_1}{k}+\lambda_0 q\right)}+\frac{q}{\omega^2+q^2}\right)e^{-y\sqrt{\frac{\Lambda_1}{\lambda_1}(\lambda_2 Msin(\theta_1)+\frac{\lambda_1}{k}+\lambda_0 q)}} \\
&-\frac{\lambda_3 Gr\ \Lambda_1\ Cos(\theta_2)\left(1-e^{-q}\right)}{\lambda_1 q^2}\frac{e^{-y\sqrt{\frac{\lambda_5 Pr\ q}{q^{\beta}(1-\alpha q^{-\alpha})^{\gamma}}}}}{\left(\frac{\lambda_5 Pr\ q}{q^{\beta}(1-\alpha q^{-\alpha})^{\gamma}}\right)-\frac{\Lambda_1}{\lambda_1}\left(\lambda_2 Msin(\theta_1)+\frac{\lambda_1}{k}+\lambda_0 q\right)} \\
&-\frac{\lambda_4 Gm\ \Lambda_1\ Cos(\theta_2)}{\lambda_1 q}\frac{e^{-y\sqrt{\frac{\lambda_6 Sc\ q}{q^{\beta}(1-\alpha q^{-\alpha})^{\gamma}}}}}{\left(\frac{\lambda_6 Sc\ q}{q^{\beta}(1-\alpha q^{-\alpha})^{\gamma}}\right)-\frac{\Lambda_1}{\lambda_1}\left(\lambda_2 Msin(\theta_1)+\frac{\lambda_1}{k}+\lambda_0 q\right)}
\end{aligned} \tag{18}$$

We used a numerical tool, the Stehfest algorithm, to examine the solution of heat and momentum fields to investigate LT's inverse. Mathematically, the Gaver Stehfest method [56–58] may be distinguished as

$$w(y,t) = \frac{ln(2)}{t}\sum_{n=1}^{N} v_n\overline{w}\left(y, n\frac{ln(2)}{t}\right)$$

where

$$v_n = (-1)^{n+\frac{N}{2}}\sum_{r=[\frac{q+1}{2}]}^{min(q,\frac{N}{2})}\frac{r^{\frac{N}{2}}(2r)!}{\left(\frac{N}{2}-r\right)!r!\ (r-1)!\ (q-r)!\ (2r-q)!}$$

To compare and confirm the findings acquired by the preceding numerical technique, we also used Tzou's method, which may be mathematically rigorous.

$$w(\xi,t) = \frac{e^{4.7}}{t}\left[\frac{1}{2}\overline{w}\left(r,\frac{4.7}{t}\right) + Re\left\{\sum_{j=1}^{N}(-1)^k\overline{w}\left(r,\frac{4.7+k\pi i}{t}\right)\right\}\right]$$

3.4. Gradients

This paper uses the following three important fundamental engineering quantities of interest: the Nusselt number, the Sherwood number, and the shear stress. These gradients are mathematically expressed as:

$$Nu = -\left.\frac{\partial T_{(y,t)}}{\partial y}\right|_{y=0} = -\mathcal{L}^{-1}\left\{\frac{\partial \overline{T}_{(0,s)}}{\partial y}\right\}, \tag{19}$$

$$Sh = -\left.\frac{\partial C_{(y,t)}}{\partial y}\right|_{y=0} = -\mathcal{L}^{-1}\left\{\frac{\partial \overline{C}_{(0,s)}}{\partial y}\right\}, \tag{20}$$

$$C_f = -\left.\frac{\partial w_{(y,t)}}{\partial y}\right|_{y=0} = -\mathcal{L}^{-1}\left\{\frac{\partial \overline{w}_{(0,s)}}{\partial y}\right\}. \tag{21}$$

4. Discussion of Results

We study the application of the recently presented Mittage–Leffler kernel called Prabhakar fractional derivative to Casson HNF (Ag-TiO_2-H_2O and Ag-TiO_2-$C_6H_9NaO_7$) and mixed convection over a vertical, inclined plate. The slip on the boundary of walls is also considered with an inclined applied magnetic field. This fractional model is solved by employing the Laplace transform scheme sustaining all initial and boundary conditions. The consequences of fractional and different involved flow parameters on energy, concentration, and momentum are consulted in Figures 2–8.

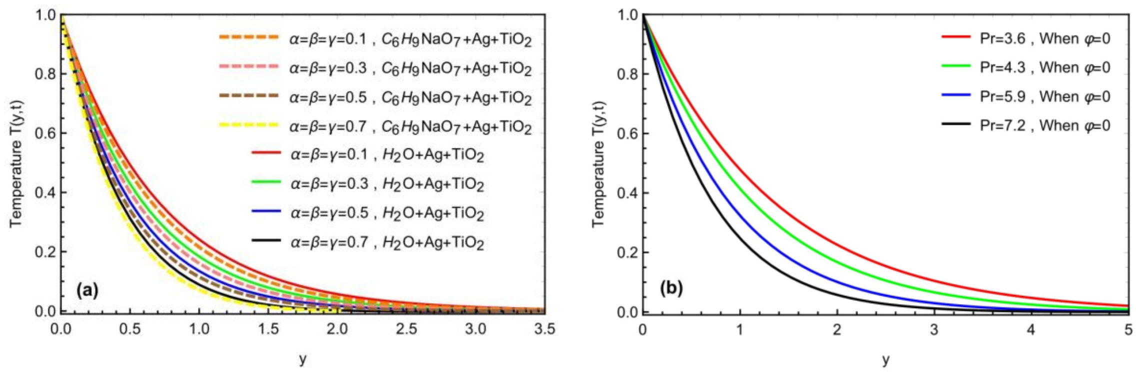

Figure 2. $T_{(y,t)}$ with the variation in (**a**) $\alpha,\ \beta,\ \gamma$ and (**b**) Pr with $\varphi = 0.02,\ t = 0.8$.

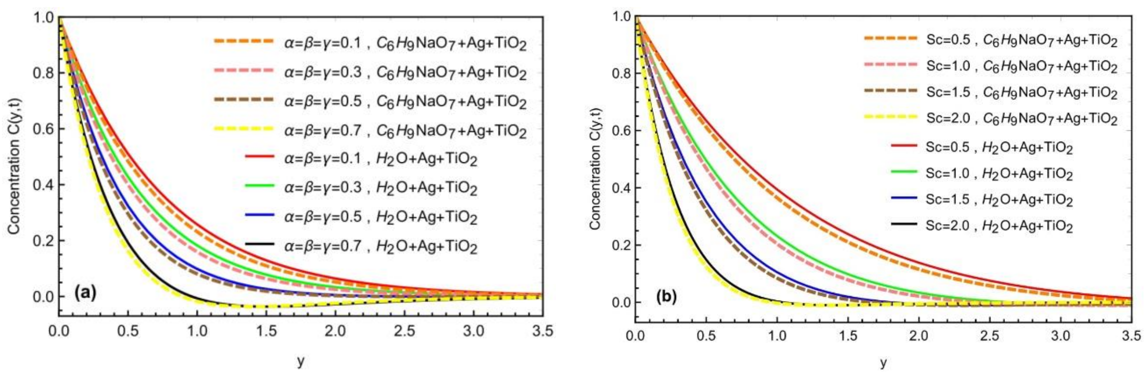

Figure 3. $C_{(y,t)}$ with the variation in (**a**) $\alpha,\ \beta,\ \gamma$ and (**b**) Sc with $\varphi = 0.02,\ t = 0.8$.

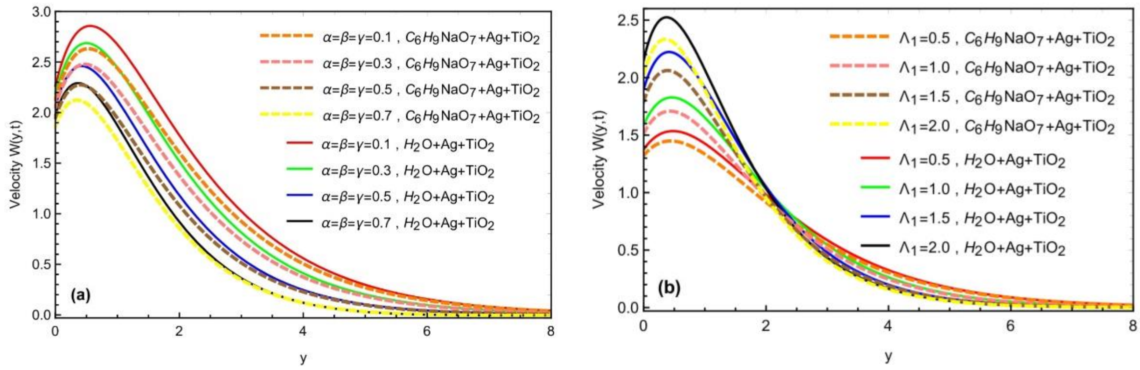

Figure 4. $w_{(y,t)}$ with the variation in (**a**) $\alpha,\ \beta,\ \gamma$ and (**b**) Λ_1 with $Pr = 7.2$, $Gr = 4.5$, $Gm = 6.7$, $h = 0.5$, $M = 1.75$, $Sc = 2.0$, $\varphi = 0.02$, $\theta_1 = \theta_2 = \frac{\pi}{4}$, $k = 0.5$, $t = 0.8$.

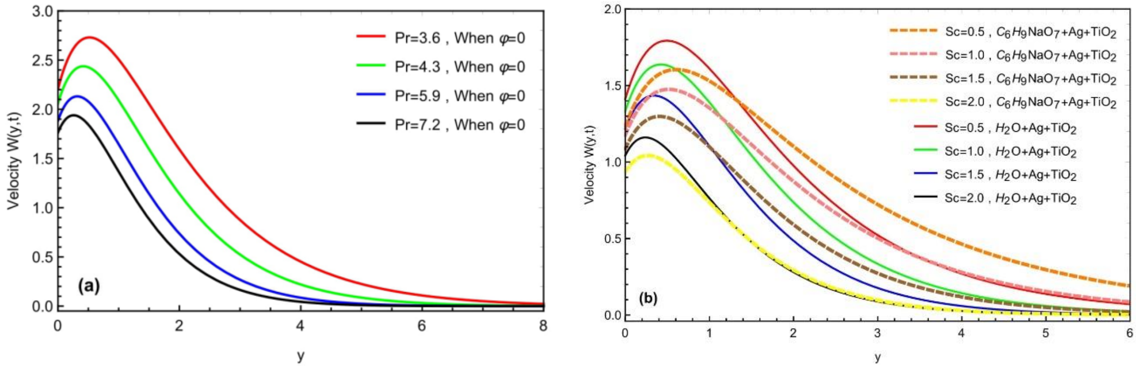

Figure 5. $w_{(y,t)}$ with the variation in (**a**) Pr and (**b**) Sc with $\alpha = \beta = \gamma = 0.8$, $Gr = 4.5$, $Gm = 6.7$, $h = 0.5$, $M = 1.75$, $\varphi = 0.02$, $\theta_1 = \theta_2 = \frac{\pi}{4}$, $k = 0.5$, $t = 0.8$.

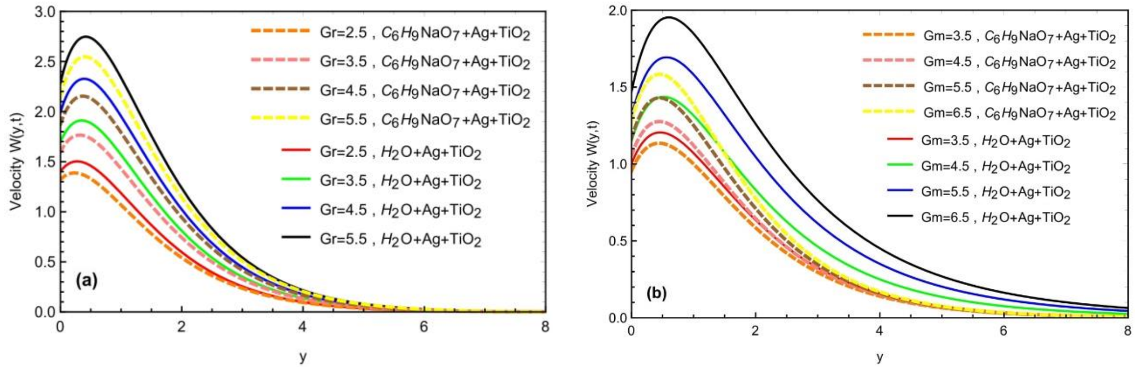

Figure 6. $w_{(y,t)}$ with the variation in (**a**) Gr and (**b**) Gm with $\alpha = \beta = \gamma = 0.8$, $Pr = 7.2$, $h = 0.5$, $M = 1.75$, $Sc = 2.0$, $\varphi = 0.02$, $\theta_1 = \theta_2 = \frac{\pi}{4}$, $k = 0.5$, $t = 0.8$.

Figure 2 is planned to see the impacts of fractional parameters $(\alpha,\ \beta,\ \gamma)$ and Pr on the temperature profile. By setting other parameters constant and varying fractional parameters and Pr, we see that the temperature rate is decayed by enhancing the $(\alpha,\ \beta,\ \gamma)$ and Pr. It means that fluid characteristics may be controlled with fractional parameters. It has been discovered that raising the fractional parameter reduces the temperature, concentration, and profiles due to the Prabhakar fractional kernel. This demonstrates the memory effect of the momentum and temperature at a certain period. Figure 2b depicts the physical influence of the Prandtl number Pr on the temperature profile while keeping the other flow parameters constant. We may argue that when the value of Pr increases, the temperature of the fluid and the thickness of the boundary layer decrease. It is primarily due to an increase in fluid viscosity and a decrease in the thermal boundary layer, which resulted in a slower fluid thermal field. Physically, when the estimations of Pr rise, which source is quickly reducing of the thermal boundary layer thickness, due to which declines the energy profile. Moreover, we perceived that the temperature for silver–titanium dioxide–sodium alginate-based HNF has a relatively more significant value than silver–titanium dioxide–water HNF.

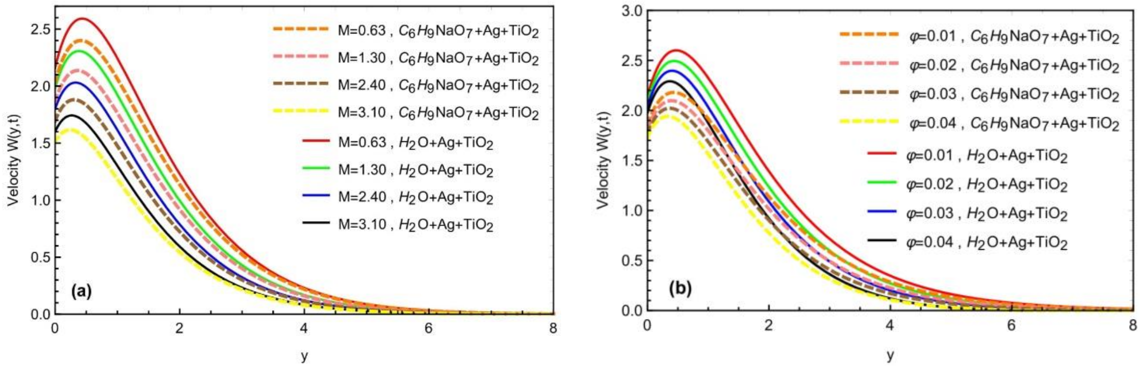

Figure 7. $w_{(y,t)}$ with the variation in (**a**) M and (**b**) φ with $\alpha = \beta = \gamma = 0.8$, $Pr = 7.2$, $Gr = 4.5$, $Gm = 6.7$, $h = 0.5$, $Sc = 2.0$, $\theta_1 = \theta_2 = \frac{\pi}{4}$, $k = 0.5$, $t = 0.8$.

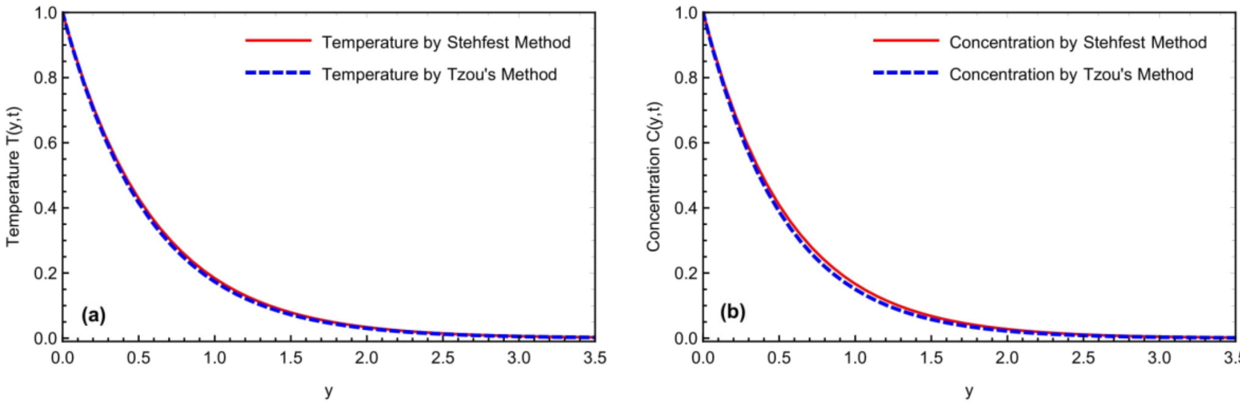

Figure 8. Comparison of (**a**) temperature and (**b**) concentration fields by numerical algorithms.

Figure 3 is planned to check the impact of (α, β, γ) and Sc on concentration. By setting other parameters fixed and vary (α, β, γ) and Sc. It is detected that concentration cannot be boosted by mean declines for a more significant estimation of (α, β, γ) and Sc. Figure 3b depicts the effect of Sc, the Schmidt number, on the concentration profile. It is clearly demonstrated that an increase in the value of the Schmidt number Sc results in a decrease in the centration profile. Because the rate of molecular diffusion decreases as Sc increases, the thickness of the boundary layer is reduced. Physically, Sc is the ratio of momentum and mass diffusivity. The fluid layers get more viscosity, so concentration declines.

Figure 4a shows that the velocity curve drops as fractional parameters are improved, and the velocity field shows a dual behavior by varying Casson parameter (Λ_1) as shown in Figure 4b. There are separate peaks for momentum profile layer thickness as well. The velocity near the plate is more incredible, but as the fluid flows away from the plate, its value decreases and becomes zero as y approaches infinity, as depicted in the figures. Figure 5a signified the influence of Pr on the velocity profile and observed that the fluid's velocity enhancements as Pr declines. The velocity layer increases thickness because of the lesser rate of thermal diffusion, Pr directs the relative viscosity of momentum boundary layers in energy transfer model problems. As predicted, raising the values of Pr lowers thermal conductivity, making the fluid thicker, and therefore reducing the thickness of the thermal boundary layer. Figure 5b displays that the velocity behavior is also seen contrary to the Sc since as the estimations of Sc increase, it drops mass diffusivity by raising the kinematic viscosity. In Figure 6a,b, we see that fluid velocity amplified for more significant estimations of thermal Grashof number (Gr) and mass Grashof number (Gm), respectively. Because Gr creates natural convection owing to buoyancy and viscosity forces acting on the fluid, large values of Gr cause buoyancy forces to increase, forcing the flow to accelerate. Physically, Gr is that it characterizes the ratio of the buoyant forces because of spatial disparity in the fluid density (produced by temperature variation) to the preventive force because of the fluid viscosity. Grashof number signifies how the buoyant force is dominant, which controls the convection because of which velocity is enlarged. A similar trend is seen for Gm. Because Gm is the ratio of viscous forces to buoyant forces owing to concentration gradient, raising the value of Gm increases fluid velocity and boundary layer thickness in both circumstances. The influence of inclined magnetic field M considered in Figure 7a shows that the velocity decays by increasing the estimation of M due to Lorentz forces. It is a type of resistant force that sources velocity decay. In Figure 7b it is realized how the volume fraction (φ) impacts the velocity. We realize that fluid velocity is reduced for great values of φ. This is physically suitable as the fluid gains much viscosity with growing φ, which sources a reduction in the fluid velocity and eventually displays the fluid motion. It is discovered that increasing the value of φ reduces the velocity. The velocity is most significant for "$\varphi = 0$" (pure water), while it is lowest for "$\varphi = 0.04$". As it rises, the viscous forces get more extraordinary, and the velocity drops. Furthermore, sodium alginate-based hybrid nanofluid is denser than pure water-based hybrid nanofluid. Figure 8a,b are planned to compare two diverse numerical approaches, Stehfest and Tzou, for temperature, concentration, and momentum profiles. The consequences from different profile curves have overlapped slightly, indicating this research work's validity. Figure 9 is designed to see the validity of our achieved results compared to Khalid et al. [59] velocity outcomes. By overlapping both curves, it is appreciated from these graphs that our attained outcomes match those developed by Khalid et al. [59]. The comparison of governed equations with different numerical schemes is analyzed in Tables 3 and 4 with nusselt number, Sherwood number, and skin friction.

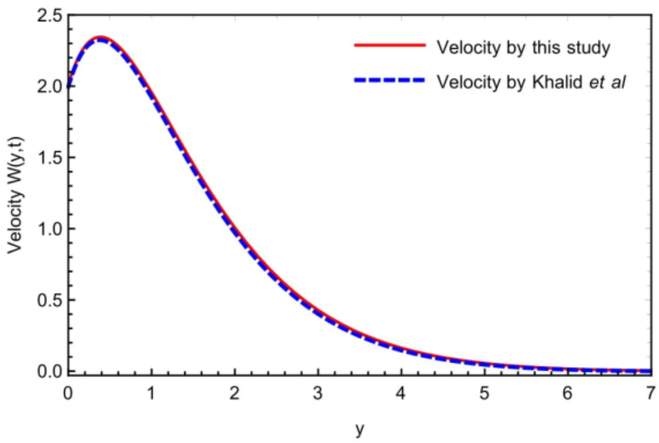

Figure 9. Comparison of velocity field with Khalid et al. [59].

Table 4. Numerical analysis of Nusselt number, Sherwood number, and skin friction.

α	Nu	Sh	C_f
0.1	1.4057	1.4801	7.5847
0.2	1.4845	1.5480	7.9900
0.3	1.5811	1.6169	8.3908
0.4	1.6826	1.6808	8.7468
0.5	1.8124	1.7340	9.0116
0.6	1.9319	1.7736	9.1780
0.7	2.0423	1.7989	9.2379
0.8	2.1374	1.8115	9.2163
0.9	2.2135	1.8123	9.1376

5. Conclusions

We investigated a Casson-type sodium alginate and water-based hybrid nanofluid combined with silver (Ag) and titanium dioxide (TiO_2) and flowing on an inclined plate in this study. The effects of an inclined applied magnetic field saturated porous plate and sinusoidal thermal conditions are also studied. The LT approach examines both governing equations' semi-analytical solutions. The behavior of various parameters is visually and quantitatively evaluated. The key findings of the graphical research are listed in bullet form below.

- With fractional and Prandtl number augmentation, both velocity and temperature fields exhibit opposing behavior.
- The memory effect is reduced for both concentration and temperature profiles by increasing the fractional value restriction.
- Because of its physical properties, the energy field fluctuates with the fluctuation in volume fractional parameters.
- The momentum profile accelerates as the Grashof number increases due to an improvement in the boundary layer of the flowing fluid.
- The permeability parameter and the applied magnetic field retorted the velocity profile for water-based hybrid nanofluid and sodium alginate nanofluid.
- The significant comparison of the momentum profile with the current physical literature adds to the study's originality.
- When comparing numerical methodologies, the curves of both methods overlap, indicating that our obtained results are legitimate.

Recent advances in the study of fractional order frameworks include the fractional natural decomposition method (FNDM), the fractional Shehu transform, and the modified generalized Taylor fractional series method (MGTFSM). Researchers in the future can correlate their findings to those we found utilizing the Caputo–Fabrizio, Atangana–Baleanu, and Prabhakar fractional methods in our investigation.

Author Contributions: Conceptualization, A.R., M.Y.A. and Q.A.; methodology, A.R. and A.U.H.; software, A.R., Q.A. and K.A.-K.; validation, A.R., I.E.S. and Q.A.; formal analysis, A.R., M.Y.A. and K.A.-K.; investigation, M.Y.A., Q.A. and A.U.H.; resources, A.R.; data curation, I.E.S.; writing—original draft preparation, A.R., Q.A. and A.U.H.; writing—review and editing, A.R., Q.A. and I.E.S.; visualization, A.R., K.A.-K. and I.E.S.; supervision, A.U.H.; project administration, I.E.S.; funding acquisition, I.E.S. and M.Y.A. All authors have read and agreed to the published version of the manuscript.

Funding: This research received no external funding.

Institutional Review Board Statement: Not applicable.

Informed Consent Statement: Not applicable.

Data Availability Statement: Not Available.

Conflicts of Interest: The authors declare no conflict of interest.

Nomenclatures

θ_1	Angle of inclination of the plate [–]
θ_2	Angle of inclination of the magnetic field [–]
g	Acceleration due to gravity $\left[LT^{-2}\right]$
C	Concentration of the fluid $\left[ML^{-3}\right]$
U_o	Constant velocity $\left[LT^{-1}\right]$
β_1	Casson fluid parameter [–]
K	Dimensionless porosity parameter [–]
μ	Dynamic viscosity $\left[ML^{-1}T^{-1}\right]$
σ	Electrical conductivity [–]
T_w	Fluids temperature at the plate $[K]$
C_w	Fluids Concentration at the plate $\left[ML^{-3}\right]$
Gr	Heat Grashof number [–]
v_f	Kinematic viscosity $\left[L^2T^{-1}\right]$
s	Laplace transformed variable [–]
Gm	Mass Grashof number [–]
D	Mass diffusion coefficient $\left[L^2T^{-1}\right]$
Nu	Nusselt number [–]
Pr	Prandtl number [–]
α, β, γ	Prabhakar fractional derivative operators [–]
k	Permeability of the porous medium [L]
Sc	Schmidt number [–]
b	Slip parameter [–]
C_f	Skin friction [–]
C_p	Specific heat at constant pressure $\left[JM^{-1}K^{-1}\right]$
t	Time $[T]$
T	Temperature $[K]$
T_∞	Temperature of fluid away from the plate $[K]$
w	Velocity $\left[LT^{-1}\right]$

Note: This [–] represents the dimensionless quantity.

References

1. Torrance, K.; Davis, R.; Eike, K.; Gill, P.; Gutman, D.; Hsui, A.; Lyons, S.; Zien, H. Cavity flows driven by buoyancy and shear. *J. Fluid Mech.* **1972**, *51*, 221–231.
2. Abu-Nada, E.; Chamkha, A.J. Mixed convection flow in a lid-driven inclined square enclosure filled with a nanofluid. *Eur. J. Mech.-B/Fluids* **2010**, *29*, 472–482.
3. Al-Salem, K.; Öztop, H.F.; Pop, I.; Varol, Y. Effects of moving lid direction on MHD mixed convection in a linearly heated cavity. *Int. J. Heat Mass Transf.* **2012**, *55*, 1103–1112.
4. Tayebi, T.; Chamkha, A.J. Effects of various configurations of an inserted corrugated conductive cylinder on MHD natural convection in a hybrid nanofluid-filled square domain. *J. Therm. Anal. Calorim.* **2021**, *143*, 1399–1411.
5. Moghadassi, A.; Ghomi, E.; Parvizian, F. A numerical study of water based Al_2O_3 and Al_2O_3–Cu hybrid nanofluid effect on forced convective heat transfer. *Int. J. Therm. Sci.* **2015**, *92*, 50–57.
6. Suresh, S.; Venkitaraj, K.; Selvakumar, P.; Chandrasekar, M. Synthesis of Al_2O_3–Cu/water hybrid nanofluids using two step method and its thermo physical properties. *Colloids Surf. A Physicochem. Eng. Asp.* **2011**, *388*, 41–48.
7. Singh, A.K.; Singh, A.; Roy, S. Analysis of mixed convection in water boundary layer flows over a moving vertical plate with variable viscosity and Prandtl number. *Int. J. Numer. Methods Heat Fluid Flow* **2019**, *29*, 602–616.
8. Govindaraj, N.; Singh, A.; Shukla, P. MHD nanofluid flow with variable physical parameters via thermal radiation: A numerical study. *Heat Transf.* **2020**, *49*, 4704–4721.
9. Gnanaprasanna, K.; Singh, A.K. A numerical approach of forced convection of Casson nanofluid flow over a vertical plate with varying viscosity and thermal conductivity. *Heat Transf.* **2022**, *51*, 6782–6800.
10. Suresh, S.; Venkitaraj, K.; Selvakumar, P.; Chandrasekar, M. Effect of Al_2O_3–Cu/water hybrid nanofluid in heat transfer. *Exp. Therm. Fluid Sci.* **2012**, *38*, 54–60.
11. Ghalambaz, M.; Doostani, A.; Izadpanahi, E.; Chamkha, A.J. Conjugate natural convection flow of Ag–MgO/water hybrid nanofluid in a square cavity. *J. Therm. Anal. Calorim.* **2020**, *139*, 2321–2336.
12. Abdel-Nour, Z.; Aissa, A.; Mebarek-Oudina, F.; Rashad, A.; Ali, H.M.; Sahnoun, M.; El Ganaoui, M. Magnetohydrodynamic natural convection of hybrid nanofluid in a porous enclosure: Numerical analysis of the entropy generation. *J. Therm. Anal. Calorim.* **2020**, *141*, 1981–1992.

13. Archana, M.; Gireesha, B.; Prasannakumara, B.; Gorla, R. Influence of nonlinear thermal radiation on rotating flow of Casson nanofluid. *Nonlinear Eng.* **2018**, *7*, 91–101.
14. Nadeem, S.; Mehmood, R.; Akbar, N.S. Oblique stagnation point flow of a Casson-nano fluid towards a stretching surface with heat transfer. *J. Comput. Theor. Nanosci.* **2014**, *11*, 1422–1432.
15. Haq, R.U.; Nadeem, S.; Khan, Z.H.; Okedayo, T.G. Convective heat transfer and MHD effects on Casson nanofluid flow over a shrinking sheet. *Cent. Eur. J. Phys.* **2014**, *12*, 862–871.
16. Alwawi, F.A.; Alkasasbeh, H.T.; Rashad, A.M.; Idris, R. A numerical approach for the heat transfer flow of carboxymethyl cellulose-water based Casson nanofluid from a solid sphere generated by mixed convection under the influence of Lorentz force. *Mathematics* **2020**, *8*, 1094.
17. Govindaraj, N.; Singh, A.K.; Roy, S.; Shukla, P. Analysis of a boundary layer flow over moving an exponentially stretching surface with variable viscosity and Prandtl number. *Heat Transf. Asian Res.* **2019**, *48*, 2736–2751.
18. Govindhasamy, I.; Singh, A.K. Boundary layer flow and stability analysis of forced convection over a diverging channel with variable properties of fluids. *Heat Transf.* **2020**, *49*, 5050–5065.
19. Patil, P.; Kulkarni, M. MHD quadratic mixed convective Eyring-Powell nanofluid flow with multiple diffusions. *Chin. J. Phys.* **2022**, *77*, 393–410.
20. Iyyappan, G.; Singh, A.K. MHD flows on irregular boundary over a diverging channel with viscous dissipation effect. *Int. J. Numer. Methods Heat Fluid Flow* **2021**, *31*, 2112–2127.
21. Patil, P.; Benawadi, S. The quadratic convective flow of Williamson nanofluid with multiple diffusions. *Phys. Scr.* **2022**, *97*, 065206.
22. Patil, P.; Benawadi, S. Shape effects on the mixed convective hybrid nanoliquid flow over a rough slender cylinder with convective condition. *Waves Random Complex Media* **2022**, *32*, 1–17.
23. Patil, P.; Shankar, H. Heat transfer attributes of Al_2O_3-Fe_3O_4/H_2O hybrid nanofluid flow over a yawed cylinder. *Propuls. Power Res.* **2022**, *11*, 416–429.
24. Fang, Z.-W.; Sun, H.-W.; Wang, H. A fast method for variable-order Caputo fractional derivative with applications to time-fractional diffusion equations. *Comput. Math. Appl.* **2020**, *80*, 1443–1458.
25. Ali, R.; Akgül, A.; Asjad, M.I. Power law memory of natural convection flow of hybrid nanofluids with constant proportional Caputo fractional derivative due to pressure gradient. *Pramana* **2020**, *94*, 131.
26. Baleanu, D.; Jajarmi, A.; Mohammadi, H.; Rezapour, S. A new study on the mathematical modelling of human liver with Caputo–Fabrizio fractional derivative. *Chaos Solitons Fractals* **2020**, *134*, 109705.
27. Ghanbari, B.; Atangana, A. A new application of fractional Atangana–Baleanu derivatives: Designing ABC-fractional masks in image processing. *Phys. A Stat. Mech. Its Appl.* **2020**, *542*, 123516.
28. Saqib, M.; Mohd Kasim, A.R.; Mohammad, N.F.; Chuan Ching, D.L.; Shafie, S. Application of fractional derivative without singular and local kernel to enhanced heat transfer in CNTs nanofluid over an inclined plate. *Symmetry* **2020**, *12*, 768.
29. Saqib, M.; Shafie, S.; Khan, I.; Chu, Y.-M.; Nisar, K.S. Symmetric MHD channel flow of nonlocal fractional model of BTF containing hybrid nanoparticles. *Symmetry* **2020**, *12*, 663.
30. Khan, U.; Zaib, A.; Ishak, A.; Elattar, S.; Eldin, S.M.; Raizah, Z.; Waini, I.; Waqas, M. Impact of Irregular Heat Sink/Source on the Wall Jet Flow and Heat Transfer in a Porous Medium Induced by a Nanofluid with Slip and Buoyancy Effects. *Symmetry* **2022**, *14*, 2212.
31. Ershkov, S.V.; Prosviryakov, E.Y.; Leshchenko, D.D. Flow of a Viscous Incompressible Fluid from a Moving Point Source. *Symmetry* **2022**, *14*, 2156.
32. Khan, A.; Jamshed, W.; Eid, M.R.; Pasha, A.A.; Tag El Din, E.S.M.; Khalifa, H.A.E.-W.; Alharbi, S.K. Unsteady Electro-Hydrodynamic Stagnating Point Flow of Hybridized Nanofluid via a Convectively Heated Enlarging (Dwindling) Surface with Velocity Slippage and Heat Generation. *Symmetry* **2022**, *14*, 2136.
33. Hayat, A.U.; Ullah, I.; Khan, H.; Weera, W.; Galal, A.M. Numerical Simulation of Entropy Optimization in Radiative Hybrid Nanofluid Flow in a Variable Features Darcy–Forchheimer Curved Surface. *Symmetry* **2022**, *14*, 2057.
34. Khan, M.S.; Siddiqui, M.A.; Afridi, M.I. Finite Difference Simulation of Nonlinear Convection in Magnetohydrodynamic Flow in the Presence of Viscous and Joule Dissipation over an Oscillating Plate. *Symmetry* **2022**, *14*, 1988.
35. Bafakeeh, O.T.; Raza, A.; Khan, S.U.; Khan, M.I.; Nasr, A.; Khedher, N.B.; Tag-Eldin, E.S.M. Physical Interpretation of Nanofluid (Copper Oxide and Silver) with Slip and Mixed Convection Effects: Applications of Fractional Derivatives. *Appl. Sci.* **2022**, *12*, 10860.
36. Sadiq, K.; Siddique, I.; Awrejcewicz, J.; Bednarek, M. Natural Convection Water/Glycerin–CNT Fractionalized Nanofluid Flow in a Channel with Isothermal and Ramped Conditions. *Nanomaterials* **2022**, *12*, 1255.
37. Raza, A.; Haq, A.U.; Farid, S. A Prabhakar fractional approach with generalized fourier law for thermal activity of non-newtonian second-grade type fluid flow: A fractional approach. *Waves Random Complex Media* **2022**, *32*, 1–17.
38. Raza, A.; Hejazi, H.A.; Khan, M.I. Impact of generalized fourier law in thermal flux convective flow over a vertical plate: Analysis of fractional derivative. *Int. J. Mod. Phys. B* **2022**, *36*, 2250162.
39. Raza, A.; Khan, U.; Zaib, A.; Weera, W.; Galal, A.M. A comparative study for fractional simulations of Casson nanofluid flow with sinusoidal and slipping boundary conditions via a fractional approach. *AIMS Math.* **2022**, *7*, 19954–19974.

40. Khan, M.I.; Mansir, I.B.; Raza, A.; Khan, S.U.; Elattar, S.; Said, H.M.; Tlili, I.; Alharbi, K.A.M.; Galal, A.M. Fractional simulations for thermal flow of hybrid nanofluid with aluminum oxide and titanium oxide nanoparticles with water and blood base fluids. *Nanotechnol. Rev.* **2022**, *11*, 2757–2767.
41. Zhang, J.; Raza, A.; Khan, U.; Ali, Q.; Zaib, A.; Weera, W.; Galal, A.M. Thermophysical Study of Oldroyd-B Hybrid Nanofluid with Sinusoidal Conditions and Permeability: A Prabhakar Fractional Approach. *Fractal Fract.* **2022**, *6*, 357.
42. Raza, A.; Hejazi, H.A.; Khan, S.U.; Khan, M.I.; Smida, K.; Tlili, I. Unsteady incompressible flow of magnetized aluminium oxide and titanium oxide nanoparticles with blood base fluid. *J. Indian Chem. Soc.* **2022**, *99*, 100568.
43. Ali, Q.; Riaz, S.; Awan, A.U. Free convection MHD flow of viscous fluid by means of damped shear and thermal flux in a vertical circular tube. *Phys. Scr.* **2020**, *95*, 095212.
44. Khan, M.I.; Raza, A.; Naseem, M.; Al-Khaled, K.; Khan, S.U.; Khan, M.I.; El-Zahar, E.R.; Malik, M. Comparative analysis for radiative slip flow of magnetized viscous fluid with mixed convection features: Atangana-Baleanu and Caputo-Fabrizio fractional simulations. *Case Stud. Therm. Eng.* **2021**, *28*, 101682.
45. Elnaqeeb, T.; Shah, N.A.; Mirza, I.A. Natural convection flows of carbon nanotubes nanofluids with Prabhakar-like thermal transport. *Math. Methods Appl. Sci.* **2020**, *10*, 1–14.
46. Shah, N.A.; Fetecau, C.; Vieru, D. Natural convection flows of Prabhakar-like fractional Maxwell fluids with generalized thermal transport. *J. Therm. Anal. Calorim.* **2021**, *143*, 2245–2258.
47. Raza, A.; Khan, U.; Zaib, A.; Mahmoud, E.E.; Weera, W.; Yahia, I.S.; Galal, A.M. Applications of Prabhakar-like Fractional Derivative for the Solution of Viscous Type Fluid with Newtonian Heating Effect. *Fractal Fract.* **2022**, *6*, 265.
48. Asjad, M.I.; Riaz, A.; Alnahdi, A.S.; Eldin, S.M. New Solutions of Fractional Jeffrey Fluid with Ternary Nanoparticles Approach. *Micromachines* **2022**, *13*, 1963.
49. Benmorsli, D.; Fellah, Z.E.A.; Belgroune, D.; Ongwen, N.O.; Ogam, E.; Depollier, C.; Fellah, M. Transient Propagation of Longitudinal and Transverse Waves in Cancellous Bone: Application of Biot Theory and Fractional Calculus. *Symmetry* **2022**, *14*, 1971.
50. Sajid, T.; Ayub, A.; Shah, S.Z.H.; Jamshed, W.; Eid, M.R.; El Din, E.S.M.T.; Irfan, R.; Hussain, S.M. Trace of Chemical Reactions Accompanied with Arrhenius Energy on Ternary Hybridity Nanofluid Past a Wedge. *Symmetry* **2022**, *14*, 1850.
51. Raza, A.; Khan, U.; Almusawa, M.; Hamali, W.; Galal, A.M. Prabhakar-fractional simulations for the exact solution of Casson-type fluid with experiencing the effects of magneto-hydrodynamics and sinusoidal thermal conditions. *Int. J. Mod. Phys. B* **2022**, *23*, 2350010.
52. Ghara, N.; Das, S.; Maji, S.; Jana, R. Effect of radiation on MHD free convection flow past an impulsively moving vertical plate with ramped wall temperature. *Am. J. Sci. Ind. Res.* **2012**, *3*, 376–386.
53. Sheikh, N.A.; Ching, D.L.C.; Khan, I.; Kumar, D.; Nisar, K.S. A new model of fractional Casson fluid based on generalized Fick's and Fourier's laws together with heat and mass transfer. *Alex. Eng. J.* **2020**, *59*, 2865–2876.
54. Asjad, M.I.; Basit, A.; Iqbal, A.; Shah, N.A. Advances in transport phenomena with nanoparticles and generalized thermal process for vertical plate. *Phys. Scr.* **2021**, *96*, 114001.
55. Garra, R.; Garrappa, R. The Prabhakar or three parameter Mittag–Leffler function: Theory and application. *Commun. Nonlinear Sci. Numer. Simul.* **2018**, *56*, 314–329.
56. Abzal, S.; Reddy, G.R.; Varma, S.V. Unsteady MHD free convection flow and mass transfer near a moving vertical plate in the presence of thermal radiation. *Ann. Fac. Eng. Hunedoara* **2011**, *9*, 29.
57. Khan, M.A.; Hammouch, Z.; Baleanu, D. Modeling the dynamics of hepatitis E via the Caputo–Fabrizio derivative. *Math. Model. Nat. Phenom.* **2019**, *14*, 311.
58. Rajesh, V. Chemical reaction and radiation effects on the transient MHD free convection flow of dissipative fluid past an infinite vertical porous plate with ramped wall temperature. *Chem. Ind. Chem. Eng. Q. CICEQ* **2011**, *17*, 189–198.
59. Khalid, A.; Khan, I.; Shafie, S. Exact solutions for unsteady free convection flow of Casson fluid over an oscillating vertical plate with constant wall temperature. *Abstr. Appl. Anal.* **2015**, *2015*, 946350.